EXPERIMENTAL AND NUMERICAL STUDIES OF FLOW AND NOISE CONTROL OF AEROFOILS USING MORPHING STRUCTURES

Qing Ai[1], **Hasan Kamliya Jawahar**[2], **Mahdi Azarpeyvand**[3] and **Carlos R. Ilário da Silva**[4]

[1] *PhD Student, Advanced Composites Centre for Science and Innovation (ACCIS), University of Bristol, Bristol, United Kingdom, BS8 1TR, qing.ai@bristol.ac.uk*

[2] *PhD Student, Department of Aerospace Engineering, University of Bristol, Bristol, United Kingdom, BS8 1TR, hasan.kj@bristol.ac.uk*

[3] *Senior Lecturer and Royal Academy of Engineering research fellow, Department of Mechanical Engineering, University of Bristol, Bristol, United Kingdom, BS8 1TR, m.azarpeyvand@bristol.ac.uk*

[4] *Technology Development Engineer, Embraer, Sáo José dos Campos, Brazil, carlos.ilario@embraer.com.br*

KEYWORD:

NACA 0012, 30P30N, morphing trailing-edge, aerofoil self-noise, slat cove filler, slat noise, LES.

ABSTRACT:

Experimental and numerical studies to characterize aerodynamic and aeroacoustic performance of simple and multi-element aerofoils using morphing structures are conducted and some preliminary results are presented here. For the simple aerofoil, a NACA 0012 aerofoil with morphing trailing-edge with deflection angle $\beta = 10°$ for a chord-based Reynolds number of $Re_c = 2.6 \times 10^5$ has been reported for two different morphing trailing-edge designs. Comprehensive flow field investigations including lift and drag forces measurements, wake profiles using hot-wire, pressure distribution along the chord and aerofoil noise emission are carried out. LES studies have been performed to further investigate the flow behaviours around aerofoils and good agreement between the experimental results and that from LES is found. For multi-element aerofoil, a parametric experimental study of MDA 30P30N multi-element aerofoil has been carried out to investigate the aerodynamic and aeroacoustic effects and efficiency of morphing structures. The study involved the use of slat cove fillers, flap cove fillers, Droop-nose configuration and slat cusp serrations. Static surface pressure measurements, unsteady surface pressure measurements using microphones and flow visualisation using particle image velocimetry (PIV) has been carried out. Results confirmed the great potential of the morphing structures, which is one of the highly sought candidate for the next generation aircraft control surfaces.

1 INTRODUCTION

MORPHING structures have received significant interest from engineering community including researchers and aviation and automobile industries, owing to their potential of high performance, low mechanism complexity and light-weight. Current high-lift systems used on aeroplane wings for example slats, aileron and trailing-edge flaps mainly consist of discrete rigid structure components which are articulated around hinges and linkages to achieve wing shape change for flow control purposes. As such, the overall system complexity and structure weight are considerably increased. Unlike conventional wing control surfaces, morphing structures for example morphing leading-edge and trailing-edge usually use the conformal structural deformation achieved through bending and twisting of structures to adaptively change wing shape, leading to simplified systems and reduced weight. Furthermore, the intrinsic continuous deformation shape and smooth structure surface in morphing structures significantly reduce airframe noise, particularly the cavity type noise and drags compared to conventional mechanical control surfaces.

Noise sources including jet noise, landing gear noise and high-lift device noise dominate the acoustic performance of an aircraft. Studies have shown that noise generated by kinetic energy scattering of turbulent eddies in the boundary layer as they cross the wing's trailing-edge becomes dominant for aeroplanes in clean configuration with projected reduction of the high-lift system noise [1]. As such, aerofoil self-noise has been considered as an important component of airframe noise during take-off and landing. Meanwhile, aerofoil self-noise has also been recognized as a key concern for wind turbines. Noise generated by wind turbines comes from both mechanical and aerodynamic sources

with the latter considered dominant [2]. Some of the currently employed passive methods for aerofoil trailing-edge noise reduction includes serrated trailing-edges [3, 4, 5, 6], porous surface treatments [7, 8, 9] and morphing trailing-edges [10]. With the use of morphing surfaces our aim is to address transition delay, separation postponement, lift enhancement, drag reduction, turbulence augmentation and noise suppression [11]. High-lift systems for aircraft wings have been widely used for lift and drag control during take-off and landing and also on wind turbine blades to increase control efficiency of the current yawing and pitching operation systems. However, high-lift devices including slats and flaps have also been identified as significant noise sources while deployed for a high-lift configuration [12]. An ideal method of morphing should achieve the control goal without affecting other goals adversely. However, in reality, continuous compromises and trade-offs have to be made for a particular design goal as it is almost impossible to decouple the interlinked flow behaviour [11], *i.e.* lift and drag forces and noise emission in the case of the high-lift systems.

Based on discussions concerning high-lift device noise sources, reduction methods have been widely proposed and studied for their potential effects. For slat slot noise reduction, slat cover cover/insert/filler, slat hook extensions and droop nose leading edges have been investigated. Horne *et al.* [13] carried out an aerocoustic investigation of a 26% Boeing 777 semi-span wing in NASA Ames 40 by 80 foot wind tunnel for noise reduction effects of a slat cover filler. Results showed that the filler used could effectively reduce slat noise emission from both outboard and inboard edges of slats and a noise reduction of up to 5 dB was observed over a broad frequency range except for a noise increase at 1200 Hz. Droop nose leading edges have received increasing interest from research community in recent years and several concepts have been experimentally investigated for noise reduction purposes. In the framework of the German R & T project HILCON, Fischer*et al.* [14] experimentally measured the integrated noise pressure level (SPL) of a droop nose leading edge design as an inboard leading edge device. Studies were carried out with an Airbus A321 as baseline and results showed that the droop nose device as an inboard leading edge can achieve a significant noise reduction of 2.4 dB in the frequency range considered compared to an A321 baseline wing. However, the maximum lift coefficient was reduced by 0.2 and stall angle of attack was decreased by 4°. Andreous *et al.* [15] also investigated effects of a drooped nose on a wing noise reduction in comparison with a slat cove filler and results showed that a droop nose was successful in removing the slat noise with a small reduction in aerodynamic performance while a filled cove only reduced the noise level by a few decibels with significant aerodynamic penalties.

The high-lift device noise sources at the chord-wise and span-wise structural discontinuities can be considered as a necessary penalty for high lift coefficients and lift-to-drag ratio in a landing configuration of aircraft. However, as demanding noise reduction goals by NASA and ACARE have further challenged the engineering community, it is essential to have a new generation high-lift systems such as morphing structures which could be incorporated in the integrated design of aeroplane wings [16].

Morphing structures have received growing interest from the engineering community, owing to their excellent mechanical and aerodynamic performance combined with light-weight. Conventional high-lift systems widely used on aeroplane wings for example ailerons and flaps use discrete parts articulated around hinges and linkages to achieve adaptive changes of wing for flow control purposes. Such a design philosophy usually leads to a heavy system of high complexity. On the contrary, morphing structures provide wing surface geometrical changes through conformal structural deformations, reducing system complexity and weight. The intrinsic continuous shape change and smooth structural surface in morphing structures can significantly reduce drag forces and noise emission [17].

Detailed experimental and computational studies have been carried out to understand the aerodynamic and aeroacoustic flow characterisation around such morphing applications and summary of some selected results of simple NACA 0012 aerofoil and multi-element 30P30N aerofoil are presented in this paper.

2 EXPERIMENTAL SETUP

Aerodynamic force measurements and wake development of a NACA 0012 aerofoil fitted with morphing trailing-edges having various camber profiles have been experimentally tested at the University of Bristol wind tunnel facilities; (i) low speed closed-circuit wind tunnel that has an octagonal working area of 2.1 m $\times$ 1.5 m $\times$ 2 m, with a contraction ratio of 3:1 and a stable working velocity range of 10 m/s to 60 m/s and (ii) open jet wind tunnel with diameter of 1.1 m, with a maximum reliable speed of 30 m/s and minimum turbulence level of 0.05%. Static pressure measurements, unsteady surface pressure fluctuation and PIV flow visualisation for the 30P30N multi-element aerofoil has been performed at the low turbulence closed-circuit wind tunnel with an octagonal working section of 0.8 m $\times$ 0.6 m $\times$ 1 m,

contraction ratio of 12:1, maximum velocity of 100 m/s and with turbulence level as low as 0.05%.

Force measurement setup: AMTI OR6-7-2000 force platform from Advanced Mechanical Technology Inc., has been used to measure the aerodynamic forces for the NACA 0012 aerofoil cases. The lift (L) and drag (D) forces were measured in the large low speed wind-tunnel where the blockage effects were found to be negligible. Two circular side-plates with a radius of 0.17 m were used to reduce the three dimensionality effects of the flow around the aerofoil. The data was sampled with a frequency of 37 Hz and sampled for a period of 30 s.

Wake measurement setup: Hot-wire measurements were made at six different streamwise locations in the wake of NACA 0012 aerofoil with morphing-trailing-edges. Dantec 55P16 single hot-wire probe was used to measure the steady flow velocities in the wake. The hot-wire probes were calibrated using a Dantec 54H10 two point mode hot-wire calibrator. The data logging frequency 40 kHz and data was collected for a time period of 20 s. The probe was mounted on a 1 m long slender cylindrical steel arm connected to the traverse system to minimise the effect of the traverse system on the aerofoil and wind tunnel. The closest point measured to the aerofoil was at 2 mm for the tested angles of attack.

2.1 Aerofoil Model Setup

2.1.1 NACA 0012 Aerofoil

RAKU-TOOL® WB-1222 polyurethane board was used to manufacture NACA 0012 aerofoil model with a chord of $c = 0.2$ m and a span of $l = 0.45$ m, which was designed to facilitate multiple interchangeable trailing-edges ($0.3c$) having different morphing camber profiles and deflection angles. Ai *et al.* [18, 19] tested the aerodynamic and aeroacoustic performance of novel morphing trailing-edge using Xfoil-BPM model. The results from the study was then used to design the morphing trailing-edge camber profiles (see Fig. 1) used in the current experimental study. The aerofoils were tested for morphing trailing-edges with varying camber profiles for deflection angles, $\beta = 10°$ (Case-1 to Case-5). A ratio between the flap length, b and tip deflection is used to define the morphing trailing-edge tip deflection angle. Case-1 represents a typical hinged flap movement and the following cases employ an increasingly cambered conformal morphing trailing-edge profiles as shown in Fig. 1.

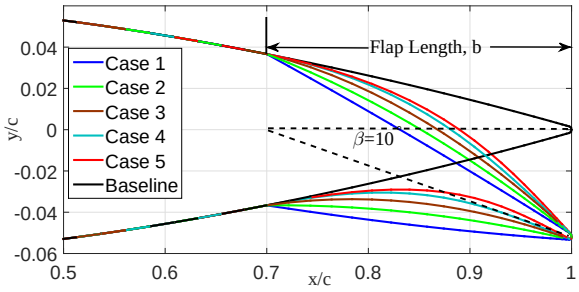

Figure 1: NACA 0012 aerofoil fitted with different morphing trailing-edges.

2.1.2 30P30N Multi-element Aerofoil

MDA 30P30N multi-element aerofoil with a retracted chord of $c = 0.35$ m and a span of $l = 0.53$ m was manufactured using 6082 aluminium alloy and machined using a computer aided numerically controlled machine. In order to maintain two-dimensionality within the slat cove and flap cove regions, no brackets were used on the spanwise direction. All the three elements were held together by steel clamps on the sides of the aerofoil. FG-3329-P07 microphones have been installed in all the three element of the wing for unsteady surface pressure measurements (see Fig. 3 & Table. 1). The FG-3329-P07 microphone has a manufacture provided sensitivity of 22.4 mV/Pa (45 Pa/V) in the flat region of the microphone response. From the calibration of the microphone installed in the wing the microphone sensitivity varied between 20.2 mV/Pa and 23.5 mV/Pa. The unsteady surface pressure measurements using FG microphones were carried out for $t = 32$ s using a sampling frequency of $f = 40$ kHz. The aerofoil has also been equipped with a large number of static pressure taps (103) placed along the mid-span of the aerofoil, which could also be used for remote sensing using microphones.

As part of the noise reduction study of three element aerofoil slat cove filler (SCF) has been designed using similar strategy followed by Imamura *et al.* [20, 21] for experimentation purposes. Initially preliminary RANS steady state simulations for the Baseline were performed for angle of attack 8°, then turbulent kinetic energy (TKE) contours were plotted and the profile with high TKE indicating the shear layer was carefully and manually extracted and was then used to plot the SCF profile. The slat cove filler (SCF) was manufactured using 3D printing technology and it was manufactured in four different sections that could be slided along the span of the slat. The SCF is fitted with 6 pressure taps along the mid-span of the wing for surface pressure measurements.

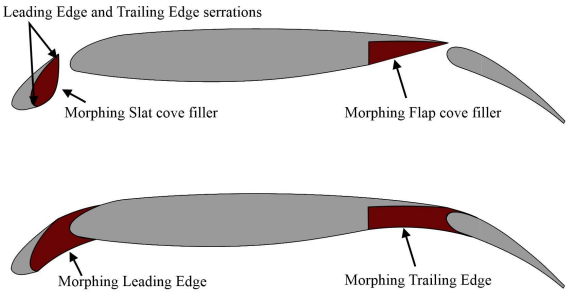

Figure 2: Morphing cove fillers for slat and flap (top) and morphing leading edge and trailing-edge.

Table 1: Microphone locations on the MDA 30P-30N aerofoil.

	No.	x (mm)	z (mm)
Main-Element	M1	22.414	277
	M2	22.414	280.6
	M3	22.414	288.4
	M4	22.414	301.4
	M5	22.414	319.6
	M6	239.701	277
Flap	F1	308.844	277
	F2	308.844	280.6
	F3	308.844	288.4
	F4	308.844	301.4
	F5	308.844	319.6
	F6	349.301	277
	F7	349.301	280.6
	F8	349.301	288.4
	F9	349.301	301.4
	F10	349.301	319.6

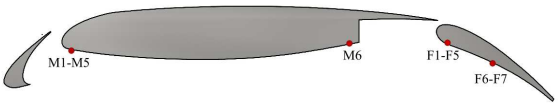

Figure 3: Microphone locations on the MDA 30P-30N aerofoil.

2.2 Computational Setup

LES studies have been carried out to investigate the flow characteristics and understand the noise reduction mechanism in morphing trailing-edges. Initially, Reynolds-averaged Navier-Stokes (RANS) numerical simulations were performed using OpenFOAM open source code and Spallart-Allmaras ($S-A$) turbulence model then the validated RANS [10] results were used to initiate the LES simulations using the same $S-A$ turbulence model. The three dimensional multi-block structured C-H type mesh was generated using commercial software ICEM-CFD. After a domain independence study the domain size was set to be $10c$ on the streamwise and crosswise direction. The domain had a spanwise thickness of $0.1c$. The cell distribution along the aerofoil was $L_x \times L_y \times L_z = 260 \times 120 \times 32$. In order to accurately capture the boundary layer the aerofoil wall was set to have a $y^+ \approx 0.5-1$. In the spanwise direction, the grid spacing was uniformly distributed corresponding to $z^+ \approx 35$. The grid along streamwise direction corresponds to a spacing of $x^+ \approx 30$ and is clustered towards the aerofoil leading-edge and trailing-edge. To capture the flow separation accurately close to the wall, the first 7 mm from the aerofoil was densely populated with 40 grid points. To capture the wake accurately the the first $1.5c$ just aft of the aerofoil was densely populated with 200 grid points. All the simulations were carried out for 20 flow through times and the data was collected for only the last 10 flow through times. A CFL value, $C_{max} \leq 1$ was maintained through out the simulations with a time step of $\Delta t = 2.75 \times 10^{-6}$ s.

3 RESULTS AND DISCUSSION

3.1 NACA 0012 Force Measurements

The lift and drag force measurements for NACA 0012 aerofoil fitted with five different types of morphing trailing-edge profiles (Case-1 to Case-5) with deflection angle, $\beta = 10°$ for flow velocity, $U_\infty = 25$ m/s, corresponding to a chord-based Reynolds number of $Re_c = 3.5 \times 10^5$ are presented in Fig. 4.

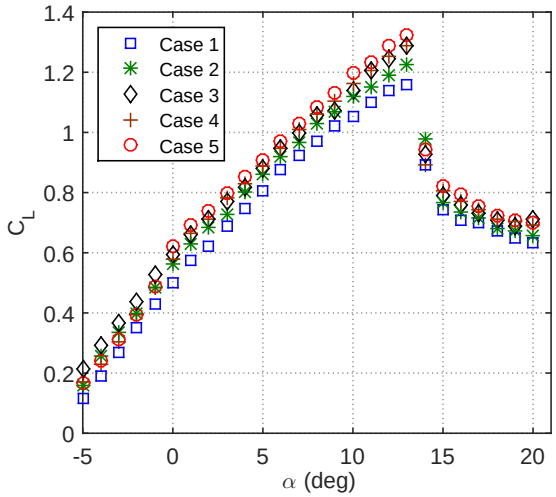

Figure 4: Lift coefficient results for NACA 0012 aerofoil fitted with various morphing trailing-edges of $\beta = 10°$, at the flow velocity of $U_\infty = 25$ m/s ($Re_c = 3.5 \times 10^5$).

The C_L results presented in Fig. 4 clearly show that the camber of the morphing trailing-edge profiles significantly affects the C_L of the aerofoil. An increase

in $C_{L,max}$ of up to 13% cab be observed for the highly cambered Case-5 compared to the simple hinged profile Case-1 just before entering stall at $\alpha = 13°$. The C_L for Case-1 with the hinged flap has the lowest $C_L - \alpha$ curve out of all the tested camber profiles. The highest C_L for angles of attack ranging from $\alpha = 0°$ to $20°$ can be seen with the highly cambered Case-5. However, at negative angles of attack, $\alpha = -5°$ to $0°$ Case-5 appears to have reduced performance close to that of Case-2. At negative angles of attack the highest C_L was achieved with morphing profile of Case-3.

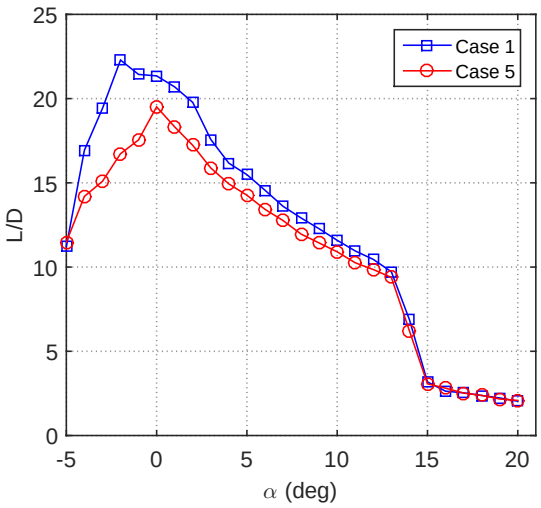

Figure 5: The lift-to-drag ratio of a NACA 0012 aerofoil fitted with morphing trailing-edge of $\beta = 10°$, at the flow velocity of $U_\infty = 25$ m/s ($Re_c = 3.5 \times 10^5$).

The lift-to-drag (L/D) ratio results of Case-1 and Case-5 are presented in Fig. 5. The results clearly show that the overall L/D ratio of Case-1 is larger than that of Case-5. The highest difference in L/D was found at negative angles of attack, $\alpha = -2°$ where the L/D of Case-1 was found to be 25% greater than that of Case-5. However, this high difference between the two cases in L/D gradually decreases as the angle of attack is increased. The L/D difference between the cases decreases to 9% at $\alpha = 0°$, 8% at $\alpha = 10°$ and to just 4% at stall angle of attack $\alpha = 13°$. Even though a large difference in C_L between Case-1 and Case-5 has been seen the stall angle of attack is not found to change as a result of morphing trailing-edge profiles and further studies are necessary further understand the post-stall properties and flow behaviour.

3.2 NACA 0012 Wake Development

LES computational studies around NACA 0012 aerofoil fitted with two morphing flap configurations, Case-1 and Case-5 has been carried out. The simulations were validated with the experiments carried out at the open-jet windtunnel facility at the University of Bristol. The validated computational results were used to further investigate the flow behaviour around the aerofoil's morphing trailing-edge and also to calculate noise levels using Curle's acoustic analogy. The LES results are validated with the experimental measurements that were captured using hot-wire anemometry at six downstream locations in the mid-span position of the aerofoil in the streamwise direction, $x = 2$ mm, 13 mm, 23 mm, 43 mm, 103 mm and 203 mm with the trailing-edge tip assumed as the datum point (x and $y = 0$) as shown in Fig. 6. The experiments and the LES were performed for angles of attack, $\alpha = 0°$, $2°$, $4°$ and $6°$ at flow velocity $U = 20$ m/s, corresponding to $Re_c = 2.6 \times 10^5$. For the purpose of brevity only angle of attack, $\alpha = 0°$ results are presented and discussed here.

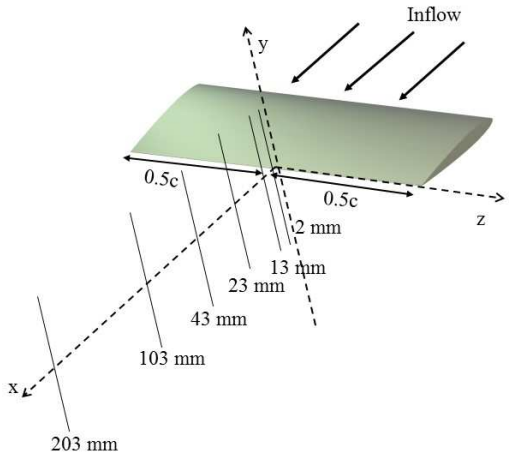

Figure 6: Chord-wise locations of flow velocity measurements in hot-wire anemometry.

The normalised mean velocity profiles at the wake for NACA 0012 aerofoil with morphing trailing-edge with deflection angle $\beta = 10°$ and angle of attack $\alpha = 0°$ are shown in Fig. 7 for flow velocity of $U_\infty = 20$ m/s, corresponding to $Re_c = 2.6 \times 10^5$. It can be observed that the LES S-A model accurately predicts the velocity deficit and peak location compared to that of the experimental data at the near-wake locations, namely $x = 2$ mm, 13 mm and 23 mm for Case-1 but slightly over predicts the velocity deficit for Case-5. At far-wake locations, $x = 43$ mm and 103 mm, the S-A model accurately predicts the velocity deficit for both the cases as seen in Fig. 7(a). The S-A model predicts the wake width to be larger than the experimental results for both Case-1 and Case-5 at far-wake location $x = 103$ mm. At far-wake location, $x = 203$ mm S-A model fails to predict

the velocity deficit, wake width and the peak location accurately for both the cases. The peak location of the experimental data sets for both the Case-1 and Case-5 have a larger flow deflection angle (flow turning angle) compared to the S-A model prediction. The S-A model's failure to accurately predict the flow at far-wake locations are mostly due to not incorporating the open-jet wind tunnels effects into the simulation.

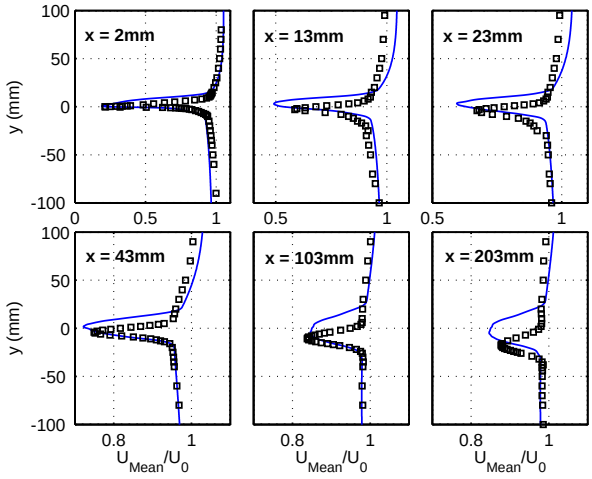

(a) CFD Case 1 —, Exp Case 1 □

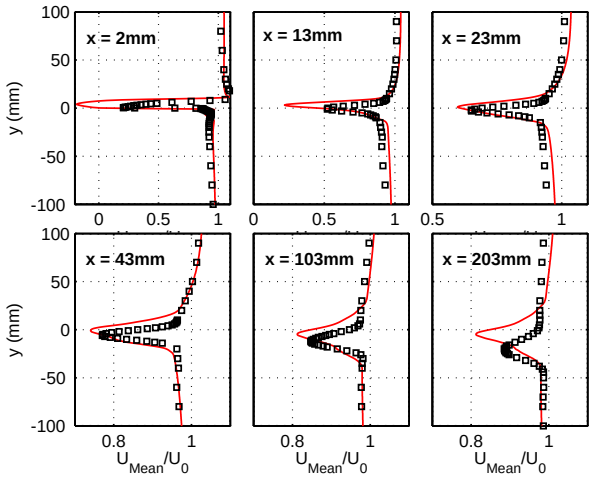

(b) CFD Case 5 —, Exp Case 5 □

Figure 7: Wake development of Case1 and Case 5 at angle of attack, $\alpha = 0^\circ$ for flow velocity $U_\infty = 20$ m/s ($Re_c = 2.6 \times 10^5$).

Iso-surfaces of Q-criterion with contours of velocity root mean squared (rms) for NACA 0012 aerofoil with morphing trailing-edge for angles of attack $\alpha = 0^\circ$ with trailing-edge deflection angle $\beta = 10^\circ$ for Case-1 and Case-5 are shown in Figs. 8(a) and 8(b) respectively. From the iso-surfaces for angle of attack $\alpha = 0^\circ$ in Fig. 8 it can be observed that for Case-1 the separation on the suction side occurs right after the flap hinge ($x \approx 0.8c$), whereas for Case-5 the separation is delayed by the smooth cambered profile and it occurs very close to the trailing-edge ($x \approx 0.9c$). For Case-1 the separation on the pressure side occurs just before the hinge of the flap ($x \approx 0.6c$) and reattaches to the surface right after the hinge ($x \approx 0.7c$) before mixing into the aerofoil wake. For Case-5 the separation on the pressure side occurs very early ($x \approx 0.6c$) and reattaches only at the very tip ($x \approx 1c$) of the trailing-edge just before separating and mixing into the aerofoil wake. This large separation with unsteady fluctuations on the pressure side between locations $x \approx 0.6c$ and $x \approx 1c$ on for Case-5 could be the primary reason for the larger wake velocity deficit compared to Case-1 as discussed in previous sections. This separation on the pressure side for Case-5 also appears to have an influence on the velocity reduction in the nearby surrounding area, which corresponds to the wider wake discussed earlier in the previous section.

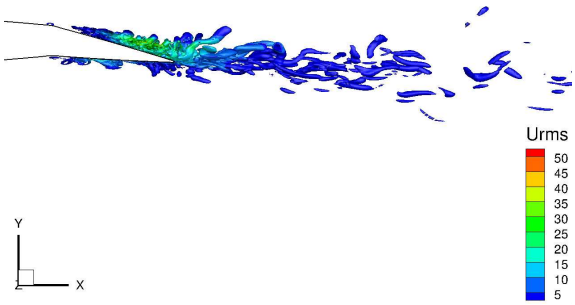

(a) Case-1

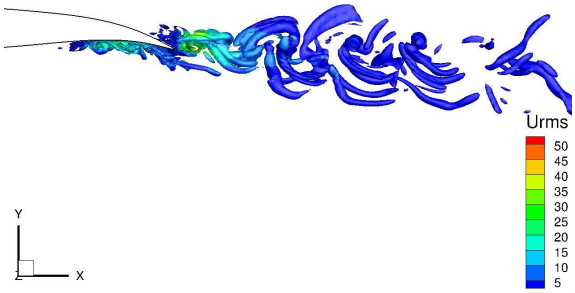

(b) Case-5

Figure 8: Iso-surfaces of Q-criterion of $Q = 1 \times 10^6 s^{-2}$ for Case-1 and Case-5 at angle of attack, $\alpha = 0^\circ$ for flow velocity $U_\infty = 20$ m/s ($Re_c = 2.6 \times 10^5$).

The sound pressure level measured at 1.2 m, 90° above the trailing-edge for Case-1 and Case-5 with deflection angle, $\beta = 10^\circ$ for angle of attack, $\alpha = 0^\circ$ calculated by Curle's acoustic analogy is presented

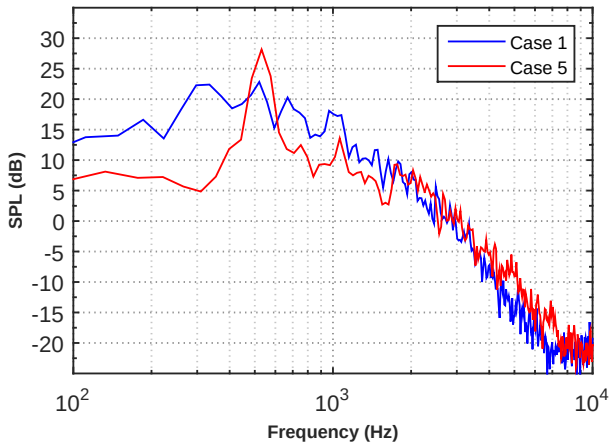

Figure 9: Sound pressure level at 1.2 m, 90° above the trailing-edge for Case-1 and Case-5 for angle of attack, $\alpha = 0°$ calculated by Curle's acoustic analogy.

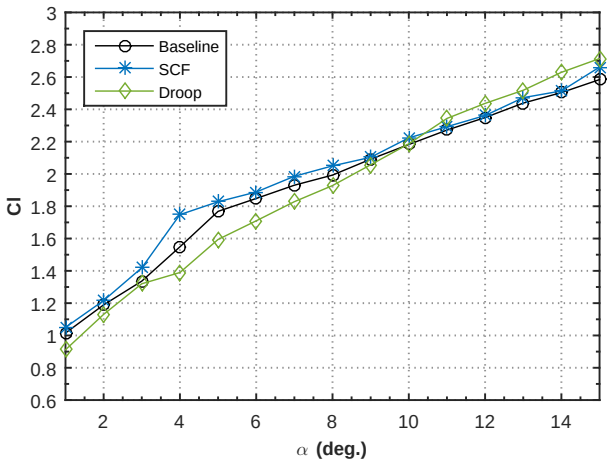

Figure 10: Coefficient of lift comparison for 30P30N aerofoil with slat modifications, for a flow velocity of $U_\infty = 47$ m/s, $Re_c = 1.1 \times 10^6$.

in Fig. 9. From the results it can be seen the noise levels are reduced for Case-5 with morphing trailing-edge compared to Case-1 with hinged flap. Noise reduction of up to 10 dB can be observed below 1000 Hz with highest noise reduction of up to 17 dB at around 300 Hz. However, a tonal peak can be observed at around 500 Hz for Case-5. The unsteady surface pressure measurements are still being studied in order to isolate the cause of this tonal noise and also to identify the noise reduction mechanism from the morphing trailing-edge Case-5.

3.3 30P30N Aerodynamic Measurements

The MDA 30P30N multi-element aerofoil with a retracted chord of $c = 0.35$ m and span of $l = 0.53$ m was tested in the low turbulence closed circuit facility at the University of Bristol. The aerofoil was tested for a wide range of angles of attack from, $\alpha = 0°$ to $\alpha = 15°$ for wide range of flow velocities 20, 30, 40 and 47 m/s for all the cases Baseline, Slat cove filler (SCF), Droop-nose and Slat cusp serrations. Even though there are 103 pressure taps on the aerofoil only a selected 64 ports were used for the measurements due to the number of ports available on the pressure scanner device. For the purpose of brevity only two angles of attack, $\alpha = 6°$ and $10°$ for a flow velocity of $U_\infty = 47$ m/s corresponding to a chord based Reynolds number of $Re_c = 1.1 \times 10^6$ are presented here. Trapezoidal integration rule was applied to the pressure coefficient C_p measurements to calculate the lift coefficient C_l for all the cases from the surface pressure measurements and are presented in Fig. 10.

The $C_l - \alpha$ curves for the reported three cases Baseline, SCF and Droop-nose are presented in Fig. 10. The results show that the slat modifications are quite sensitive to angle of attack. At $\alpha = 4°$ it can be seen that SCF configuration produces much higher C_l compared to Baseline. But after $\alpha = 6°$ the difference in C_l between the Baseline and SCF are very minimal. Droop-nose produces lesser lift compared to the other two cases between angles of attack $\alpha = 4°$ and $8°$ with higher percentage of lift reduction found at lower angles of attack. This is due to a very high leading edge deflection angle of the Droop-nose for such low angles of attack. However, at high angles of attack $\alpha = 11°$ to $15°$ Droop-nose has a higher C_l than the Baseline and SCF cases.

Figures 11 and 12 show the pressure coefficient C_p calculated from the mean surface pressure measurements acquired along the mid-span for Baseline, SCF and Droop noise configurations. The presented results are for selected angles of attack, $\alpha = 6°$ and $10°$ for a chord based Reynolds number of $Re_c = 1.1 \times 10^6$. The results on the slat in Fig. 12 show that the C_p on the pressure side remains unchanged for Baseline between both the presented angles of attack. But the C_p for the SCF changes quite significantly on the pressure side for $\alpha = 6°$ and $10°$. The results in Fig. 11 show that the modifications on the slat such as SCF affect the suction peak on the main-element of the aerofoil. Baseline has the highest suction peak for both the presented angles of attack. The suction peak on the main-element for the SCF are almost the same for both the angles of attack whereas for Baseline the suction peak increases with α and has a value of $C_p = -4.5$ and -5 for angle of attack, $\alpha = 6°$ and $= 10°$ respectively. The Droop-nose modification by combining the slat and main-element of the aerofoil results in completely different C_p distribution compared to the Baseline and SCF as seen in Figs. 11 and 12. At $\alpha = 6°$ the Droop-nose configuration does not create any lift on the very

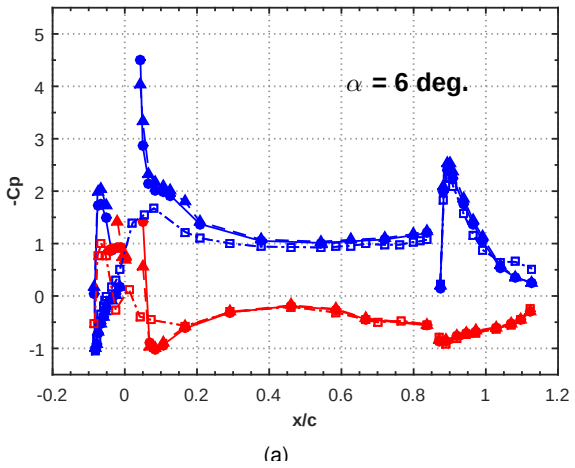

(a)

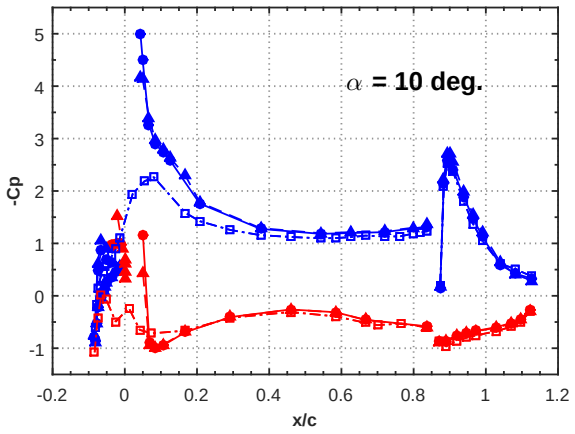

(b)

Figure 11: Coefficient of pressure distribution over 30P30N aerofoil with slat modifications, for a flow velocity of $U_\infty = 47$ m/s, $Re_c = 1.1 \times 10^6$.
Suction side — and Pressure side — for Baseline: Circles with solid lines; Slat Cove Filler: Triangles with dashed lines; Droop-nose: Squares with dotted-dashed lines.

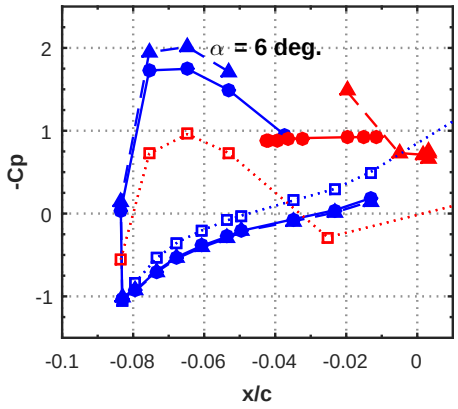

(a)

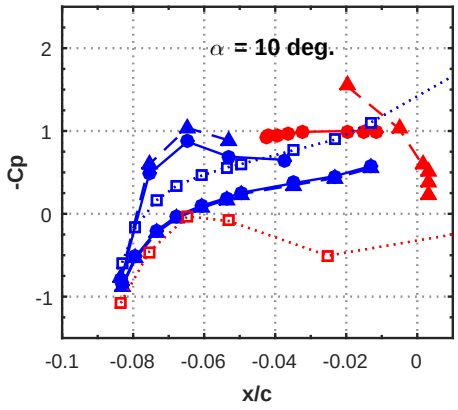

(b)

Figure 12: Coefficient of pressure distribution over 30P30N aerofoil with slat modifications around the slat region, for a flow velocity of $U_\infty = 47$ m/s, $Re_c = 1.1 \times 10^6$.
Suction side — and Pressure side — for Baseline: Circles with solid lines; Slat Cove Filler: Triangles with dashed lines; Droop-nose: Squares with dotted-dashed lines.

leading edge ($\approx -0.02c$) due to the high angle of deflection (30°) of the leading edge at such low angle of attack. However, as the angle of attack is increased Droop-nose configuration produces lift. The suction peak over Droop-nose at the same chord locations as that of the Baseline and the SCF case are drastically reduced (40%) due to the absence of the re-energized flow that passes through the slat gap over the main-element. The C_p measurement over the flap for all the reported three cases does not change for a given angle of attack. The changes to the slat for the tested Reynolds number ($Re_c = 1.1 \times 10^6$) and angle of attacks (6°&10°) appears to not affect the separation on the flap. Previous studies on 30P30N aerofoil has shown that the confluent boundary layers arising from the slat and main-element plays a major role on the delayed separation over the flap.

3.4 30P30N Acoustic Characteristics

The unsteady surface pressure measurements have been acquired for 21 microphones placed on the aerofoil at locations that are detailed in Fig. 3 and Table. 1. For the purpose of brevity only the microphones M1 and M6 on the main-element for angles of attack, $\alpha = 6°$ and 10° for $Re_c = 1.1 \times 10^6$ are presented and discussed here. The results from the unsteady surface pressure measurements at location M1 on the leading edge of the main-element are shown in Fig. 13. The results are not available for the Droop-nose configuration for this location as the microphones were covered by the Droop-nose profile. The noise results clearly shows tonal peaks for the Baseline cases at both the angles of attack with varying noise intensities for different angles of attack. For the reported results three distinct peak for $\alpha = 6°$ with noise levels of 110 dB, 95 dB and

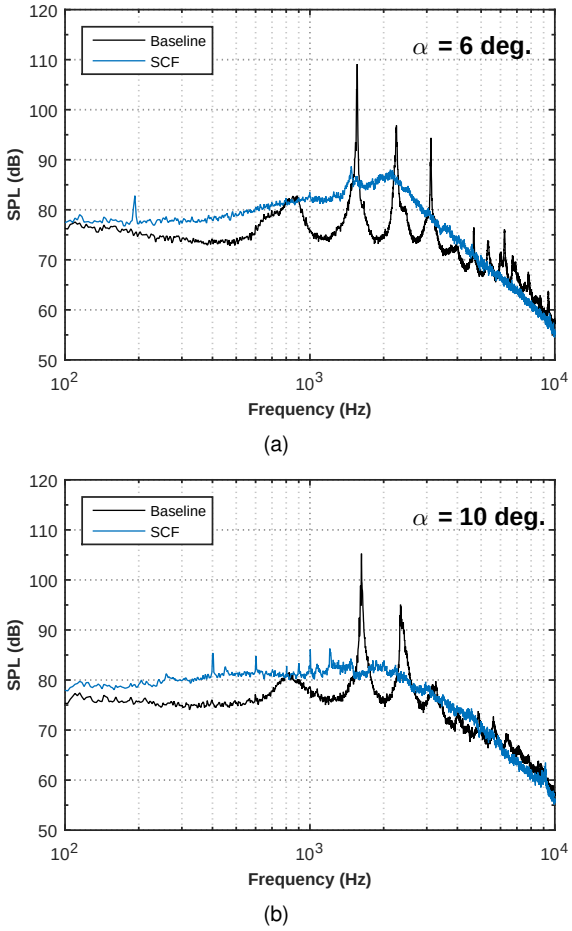

Figure 13: Pressure fluctuation spectra for surface microphone M1 ($x = 0.064c$) at main-element leading-edge of a 30P30N aerofoil with slat modifications, for a flow velocity of $U_\infty = 47$ m/s, $Re_c = 1.1 \times 10^6$.

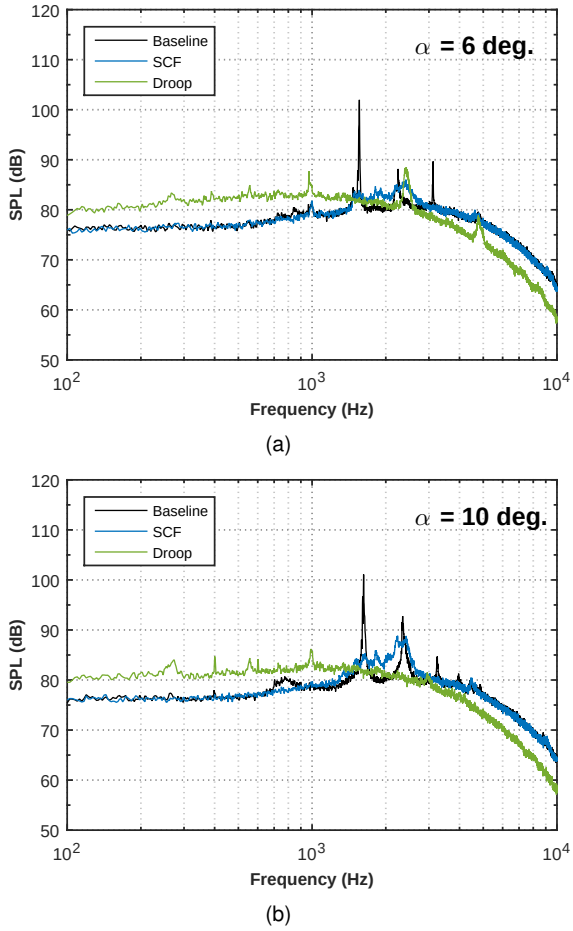

Figure 14: Pressure fluctuation spectra for surface microphone M6 ($x = 0.68c$) at main-element trailing-edge of a 30P30N aerofoil with slat modifications, for a flow velocity of $U_\infty = 47$ m/s, $Re_c = 1.1 \times 10^6$.

93 dB at frequencies 1050 Hz, 1150 Hz and 1200 Hz respectively are observed. At $\alpha = 10°$ only two distinct tonal peaks with nose levels of 95 dB and 93 dB at frequencies 1050 Hz and 1150 Hz are observed. This tonal peak is completely eliminated for SCF case for both the angles of attack with an increase in broadband noise of upto 5 dB. The reason behind the increase in broadband noise and methods to reduce them are still being investigated through detail analysis of unsteady surface pressure measurements and PIV studies.

The unsteady surface pressure fluctuation at the microphones on the trailing-edge of the main-element are shown in Fig. 14. Unlike the multiple tonal peaks observed in the microphone location M1 only a single tonal peak of 100 dB are seen in both the angles of attack. The results here do not show a overall increase in broadband noise for the SCF case compared to the Baseline as seen in the microphone location M1 on the leading-edge of the main-element wing. Even though, the Droop-nose configuration has shown complete elimination of the tonal noise behaviour it shows a increase of upto 5 dB in noise below 1000 Hz for both the angles of attack.

3.5 30P30N Flow Visualisation

Particle image velocimetry (PIV) has been carried out around the slat region for 30P30N multi-element aerofoil for angles of attack $\alpha = 6°$ and $10°$ for flow velocities of $U_\infty = 47$ m/s, corresponding to $Re_c = 1.1 \times 10^6$. Figures 15 and 16 show the mean velocity distribution around the slat region with streamlines showing the flow direction for two cases Baseline and SCF for angles of attack $\alpha = 6°$ and $10°$. For the Baseline it can be seen that the shape of the fixed vortices that is present within the slat gap is of different shape and structure. For the Baseline with $\alpha = 6°$ the vortices appears slightly larger than that of the $\alpha =$

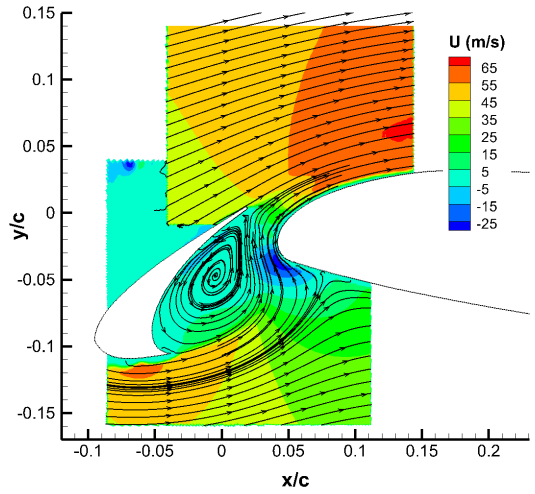

(a) $\alpha = 6°$

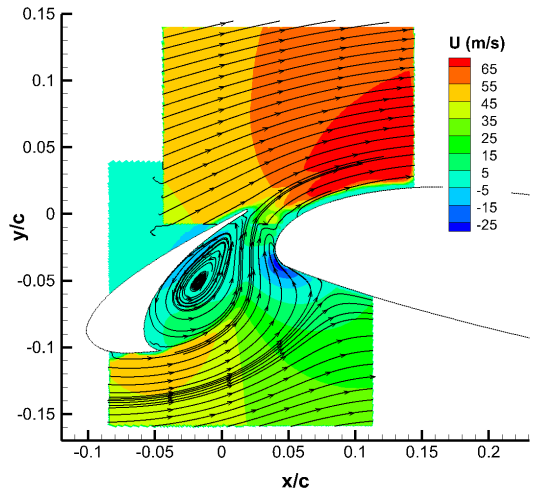

(b) $\alpha = 10°$

Figure 15: PIV flow visualisation around slat region for 30P30N Baseline aerofoil a flow velocity of U_∞ = 47 m/s, $Re_c = 1.1 \times 10^6$.

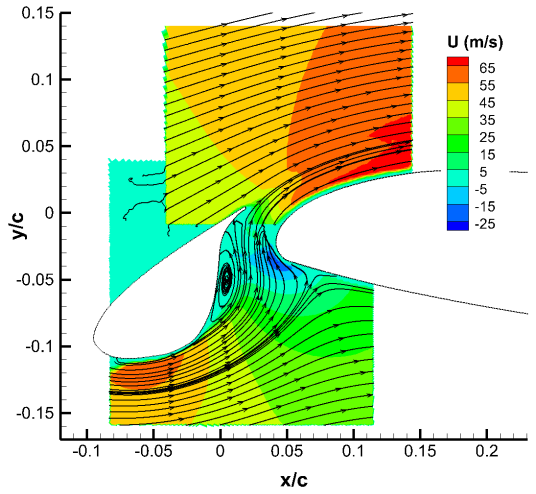

(a) $\alpha = 6°$

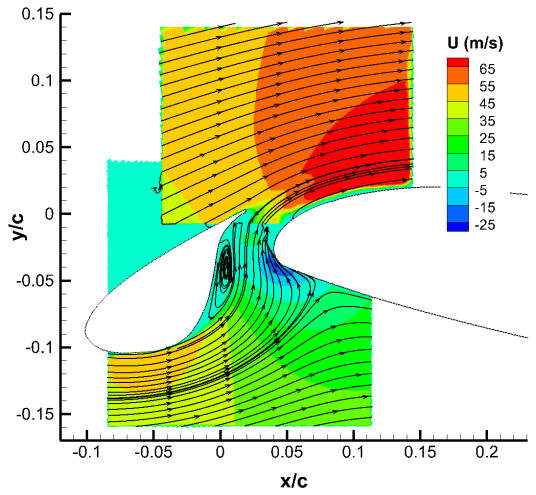

(b) $\alpha = 10°$

Figure 16: PIV flow visualisation around slat region for 30P30N aerofoil with SCF for a flow velocity of U_∞ = 47 m/s, $Re_c = 1.1 \times 10^6$.

10°. This is because as angle of attack is increased the stagnation point on the slat pressure side moves away from the slat trailing-edge towards the cusp. The SCF case eliminates this large vortices and give rise to another smaller vortices. The fixed vortices observed in the Baseline can be related to the tonal peaks that were observed at M1 surface microphone. The use of SCF eliminates this fixed vortex thus eliminating the tonal peaks. This corresponds to the noise reduction observed earlier from the unsteady surface microphone measurements.

4 CONCLUSION

The aerodynamic and aeroacoustic performances of morphing structures on a simple and multi-element aerofoil has be investigated using experimental and numerical techniques. For the simple aerofoil, NACA 0012 aerofoil with chord of $c = 0.2$ m and span of $l = 0.45$ m fitted with morphing trailing-edge with a deflection angle of $\beta = 10°$ was tested for a wide range of angles of attack, $\alpha = -5°$ to 20°. The aerofoil was tested for a flow velocity of $U_\infty = 20$ m/s corresponding to a chord based $Re_c = 2.6 \times 10^5$. The aerodynamic force measurements has shown that morphing trailing-edge with highly cambered profile (Case-5) produces higher lift than that of simple hinged flap profile (Case-

1). Hot-wire measurements at six different wake locations for $\alpha = 0^\circ$ has been made to understand aerodynamic characteristics of the morphing trailing-edge. Detailed LES using S-A turbulence model has been carried out and validated with the experimental results. The validated LES results has been used to visualise the flow structure and the unsteady surface pressure measurements has been used with Curle's analogy to calculate far-field noise. The noise measurements has showed upto 10 dB of noise reduction for Case-5. For the multi-element aerofoil, MDA 30P30N aerofoil with a retracted chord of $c = 0.35$ m and span of $l = 0.53$ m has been experimentally tested and reported for three different configurations Baseline, SCF and Droop-nose. Static surface pressure measurements, Unsteady surface pressure measurements using microphones and PIV measurements were carried out as part of the experimental campaign and only results for two angles of attack $\alpha = 6^\circ$ and $\alpha = 10^\circ$. The C_p measurements show very close lift characteristics between the Baseline and SCF cases. However, in the case of C_l calculations the SCF profile is sensitive at low angles of attack. The Droop-nose configuration has a different aerodynamic characteristics compared to the other two cases. At low angles of attack it exhibits lower lift characteristics but at higher angles of attack it has slightly better lift characteristics compared to the other two cases. The unsteady surface pressure at microphone location M1 on the main-element for the Baseline shows multiple tonal peak behaviour. This tonal peak has been completely eliminated by the use of SCF but it increased the overall broadband noise by about 5 dB. The PIV results showed a large fixed vortices present within the slat-cove region for both the angles of attack, which was eliminated by the use of SCF. The presence and elimination of the vortices also correspond to the presence and elimination of the tonal peak observed in the unsteady surface microphone measurements. The results from the application of morphing structures to both the simple and multi-element has showed improvement in aerodynamic and aeroacoustic characteristics for both the types of aerofoil.

5 REFERENCES

[1] Lockard, D.P., Lilley, G.M., *The Airframe Noise Reduction Challenge*, 2004, NASA/TM-2004-213013.

[2] Wagner S., Bareriss R., Guidati G. *Wind Turbine Noise*; Springer:Berlin,1996;67-92.

[3] Liu, X., Azarpeyvand, M., and Theunissen, R., "On the Aerodynamic Performance of Serrated aerofoils," 22nd International Congress on Sound and Vibration, pp. 1–16, Florence, italy, 2015.

[4] Liu, X., Kamliya Jawahar, H., Azarpeyvand, M., and Theunissen, R., "Aerodynamic and Aeroacoustic Performance of Serrated aerofoils," 21st AIAA/CEAS Aeroacoustics Conference, pp. 1–16, Dallas, TX, 2015.

[5] Liu, X., Kamliya Jawahar, H., Azarpeyvand, M., and Theunissen, R., "Wake Development of aerofoils with Serrated Trailing Edges," 22nd AIAA/CEAS Aeroacoustics Conference, pp. 1–21, 2016.

[6] Lyu, B., Azarpeyvand, M., and Sinayoko, S., "Prediction of noise from serrated trailing-edges", Journal of Fluid Mechanics, Vol. 793, 2016, pp. 556–588.

[7] Liu, H.R., Azarpeyvand, M., Wei, J.J., Qu, Z.G., "Tandem cylinder aerodynamic sound control using porous coating", Journal of Sound and Vibration, 334 (2015), pp. 190–201

[8] Showkat Ali, S. A., Liu, X., and Azarpeyvand, M., "Bluff Body Flow and Noise Control Using Porous Media," 22nd AIAA/CEAS Aeroacoustics Conference, 2016.

[9] Showkat Ali, S. A., Szoke, M., Azarpeyvand, M., and Ilario, C., "trailing-edge Bluntness Flow and Noise Control Using Porous Treatments," 22nd AIAA/CEAS Aeroacoustics Conference, 2016.

[10] Ai, Q., Kamliya Jawahar, H., Azarpeyvand, M., "Experimental investigation of aerodynamic performance of aerofoils fitted with morphing trailing-edges", *54th AIAA Aerospace Sciences Meeting, AIAA SciTech*, pp. 1–12, San Diego, California., 4-8, January, 2016.

[11] Gad-el-Hak, M. *Flow Control: Passive, Active, and Reactive Flow Management*; Cambridge University Press: New York, 2006.

[12] Brand. C.B, Seume, J.R. Flaps for wind turbine applications: results of an acoustic study. *the European Wind Energy Association 2015 Annual Event*, Paris, France, 17-20 Nov 2015.

[13] Horne,W.C., James, K.D., Arledge, T.K., Soderman, P.T., Burnside, N., Jaeger, S.M. Measurements of 26% 777 airframe noise in the NASA Ames 40 by 80 foot wind tunnel. *the 11th AIAA/CEAS Aeroacoustics Conference (26th AIAA Aeroacoustics Conference)*, Monterey, California, USA, 23-25 May 2005. AIAA-2005-2810.

[14] Fischer, M., Friedel, H., Holthusen, H., Golling, B., Emunds, R. Low noise design trends derived from wind tunnel testing on advanced high-lift

devices, *12th AIAA/CEAS Aeroacoustics Conference (27th AIAA Aeroacoustics Conference)*, Paper No. AIAA 2006-2562, 8 - 10 May 2006, Cambridge, Massachusetts. DOI: 10.2514/6.2006-2562.

[15] Andreous, C., Graham, W., Shin, H. Aeroacoustic comparison of aerofoil leading edge high-lift geometries and supports. *the 45th AIAA Aerospace Sciences Meeting and Exhibit*, Reno, Nevada, USA, 8-11 Jan, 2007. AIAA 2007-230.

[16] Advisory Council for Aviation Research ans Innovation in Europe, *Strategic Research and Innovation Agenda Executive Summary*, online, http://www.acare4europe.com/sria/exec-summary/volume-1, [Last seen on May 08, 2015].

[17] Dobrzynski W. Almost 40 years of airframe noise research: what did we achieve?. *Journal of Aircraft* 2010; **47**:353-367.

[18] Ai, Q., Azarpeyvand, M., Lachenal, X., Weaver, P., "Aerodynamic and Aeroacoustic Performance of aerofoils Using Morphing Structures ", *Wind Energy*, First published online: 16 September 2015,

[19] Ai, Q., Azarpeyvand, M., Lachenal, X., Weaver, P., "Airfoil Noise Reduction Using Morphing trailing-edge", *The 21st International Congress on Sound and Vibration*, pp. 1–8, Beijing, China., 13-17, July, 2014.

[20] Imamura, T. et al., "Designing of Slat Cove Filler as a Noise Reduction Device for Leading-edge Slat", *13th AIAA/CEAS Aeroacoustics Conference (28th AIAA Aeroacoustics Conference)*., pp. 1–17, Rome, Italy, 2007.

[21] Ura, H. et al., "Investigation of Airframe Noise from High Lift Configuration Model", *46th AIAA Aerospace Sciences Meeting and Exhibit*.,pp. 1–16, January. Reno, NV, 2008.